ESKİŞEHİR TECHNICAL UNIVERSITY JOURNAL OF SCIENCE AND TECHNOLOGY
A- APPLIED SCIENCES AND ENGINEERING

2018, 19(4), pp. 815 - 830, DOI: 10.18038/aubtda.413304

IMPLEMENTATION OF LONG-PERIOD FIBER GRATINGS FOR REFRACTIVE INDEX MEASUREMENT OF LIQUIDS

Cansu İDE [1] , Kıvılcım Yüksel ALDOĞAN [1, *]

[1] Electrical - Electronics Engineering Department, İzmir Institute of Technology, 35430, İzmir, Turkey

ABSTRACT

Refractive index (RI) is one of the optical parameters that is of paramount interest in characterizing liquid solutions and solvents. Increased public awareness and legal requirements for quality standards in different sectors have created a need for reliable, fast, automated, remote and/or portable refractive index sensors with multi-measurement capability. The fiber-based RI sensors are very good candidates in providing attractive solutions in such application areas and have been attracting a growing interest by the scientific community. In this work, a fiber optic refractive index sensor has been investigated. It uses a long-period fiber grating (LPFG) and an Optical Spectrum Analyzer (OSA), as sensor head and interrogator unit, respectively. New measurements of refractive indices of common solvents and solutions at the low-loss telecom wavelength band have been successfully demonstrated by using the proposed sensor. The reported measurement results are in excellent agreement with our simulation results and reference measurements realized by conventional measurement techniques.

Keywords: Fiber optic sensor, Long-period fiber grating, Refractive index measurement

1. INTRODUCTION

Refractive index (RI) is considered as one of the physical properties of material such as boiling point, melting point and density. The measurement of RI is frequently used in a variety of fields, such as chemical industry, food quality and safety analysis, bio-medical applications, environmental imaging systems, petroleum and oil industry and material analysis. There is an increasing interest in recent years in determining the exact value of the refractive index of the materials as it is a critical parameter in all aforementioned areas. During the last thirty years, several research groups have published different types of fiber-based refractive index sensors. These sensors include fiber Bragg gratings (FBG), long period gratings (LPGs) in a simple or tapered fiber structures, photonic crystal fibers (PCF), micro-interferometers and sensors using surface Plasmon resonance (SPR) effects [1–3].

In this study, we focused on the long-period fiber grating (LPFG) based-refractometers inscribed into standard single mode fiber. They are compact and do not require the use of specialty fibers, side polishing fibers and/or post processing. They can be used directly to measure the change in the refractive index of the surrounding medium due to the cladding modes based coupling mechanism. And they may be as sensitive as SPR based refractive index sensors with some sensitivity enhancement methods [4–7].

In the framework of this work, we first of all, studied the operation principles of LPFG including the modelling aspects of this sensing element. For this purpose, transmission spectra of LPFGs to the external refractive index changes have been simulated by employing the two-layer geometry. Then, experimental work has been realized on different concentrations of glucose-water, glycerol-water solutions, and various chemicals. Our experimental results show an excellent agreement with the theory which demonstrated the capability of measuring RI of liquids in the telecommunication wavelength range.

*Corresponding Author: kivilcimyuksel@iyte.edu.tr
Received: 09.04.2018 Accepted: 15.10.2018

2. MATERIALS AND METHODS

Fiber gratings can be fabricated by creating a periodic refractive index modulation in the fiber with different methods, such as; applying mechanical or thermal stress, ultraviolet (UV) irradiation or etching the cladding. In a LPFG, coupling occurs between the core mode (i.e. LP_{01} or HE_{11}) and the cladding modes (i.e. LP_{0m} or HE_{1m} with m = 1, 2, 3…) propagating in the same direction [8]. When the light traveling in the core couples to the cladding modes, intensity of it decays due to scattering losses, leaving attenuation bands in the transmission spectrum of the fundamental core mode.

Therefore, the transmission spectrum of the long period fiber grating has a series of attenuation bands near the resonant wavelengths, which satisfy the phase matching condition [9]:

$$\lambda_{res} = \left(n_{eff\_co} - n^{m}_{eff\_cl}\right)\Lambda \tag{1}$$

where λ_{res} is the resonant wavelength, n_{eff_co} is the effective refractive index of the core mode, $n^{m}_{eff\_cl}$ is the effective refractive index of the m^{th} cladding mode, and Λ is the grating period.

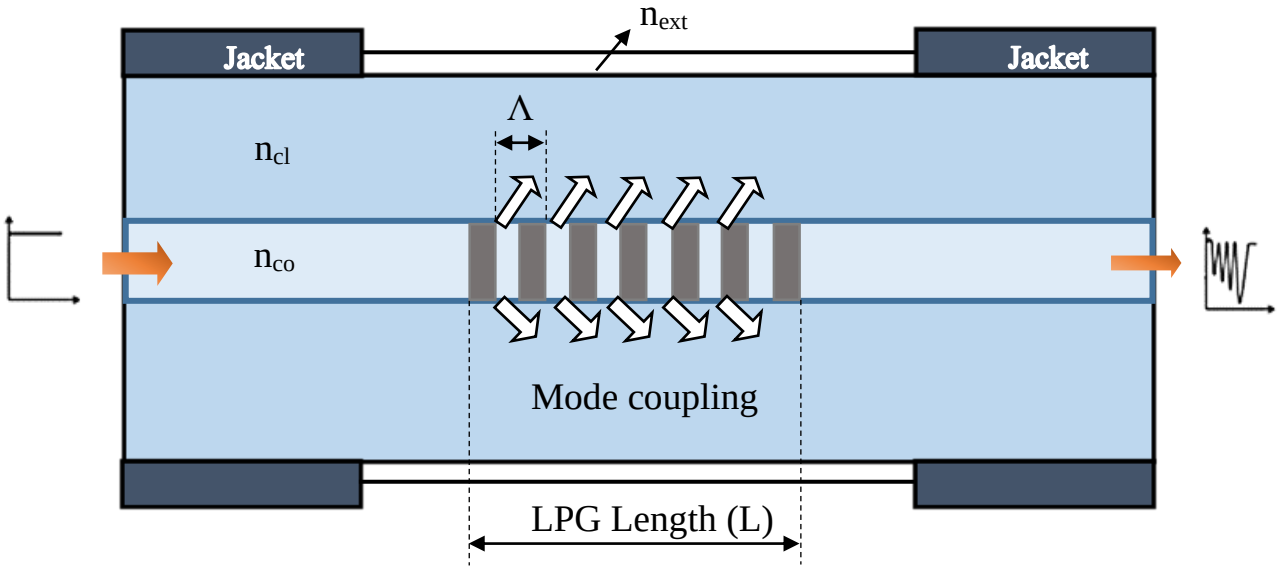

Figure 1. Coupling of a fundamental core mode to cladding modes in a long-period fiber grating [10].

Effective refractive index of the cladding depends on the refractive index of the external medium. Therefore, any variation in refractive index of the external medium may cause a wavelength shift in the transmission spectrum compared to its initial value. With the help of this spectral shifts, LPFGs can be used as refractive index sensors.

2.1. Simulation Procedures

The modelling of LPG transmission spectra is a complex calculation. There are two approaches for computer modelling: two-layer model [11], and three-layer model [8, 12]. Both methods are based on coupled mode theory (CMT) and both methods use the weakly guided approximation in order to avoid complex expressions in the definite mode solutions. In the two-layer fiber geometry (shown in Figure 2 (a)), the effect of the core is assumed to be negligible at the cladding ambient interface when determining the cladding effective refractive index. On the other hand, in the three-layer model (shown in Figure 2 (b)), the effect of the core is incorporated in the calculations [12].

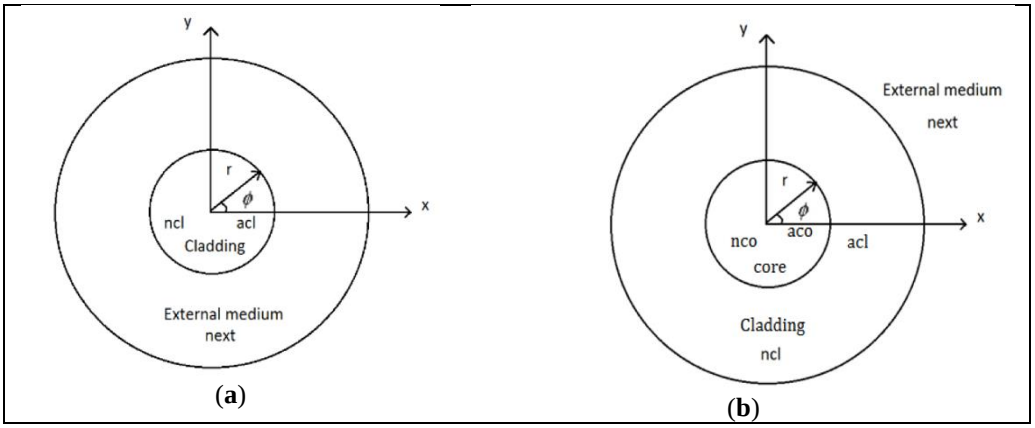

Figure 2. (a) Two-layer model; (b) Three-layer model cross sectional views of an optical fiber when calculating various cladding modes.

In this study, the necessary steps to determine the transmission spectrum of the LPFG used in the experiments were reproduced by using the two-layer model due to its relatively easy implementation in terms of coding and computational resources.

The MATLAB codes consist of a series of sub-procedures (for the program flow-chart cf. Figure 4). In the simplest terms, the simulation procedure steps are as follows:

1. Calculation of the propagation constants of the fundamental and cladding modes,
2. Determining the effective refractive indices of the core and cladding modes,
3. Calculation of the coupling coefficient for coupling between specific modes,
4. Finally, obtaining the complete transmission spectrum by using the coupled-mode theory.

These four steps providing the backbone of the theoretical part of the work are explained in the following sub-sections.

2.1.1. Determining the effective refractive indices of modes

2.1.1.1. Effective refractive index of core

Based on the weakly guided approximation, the fundamental core mode can be defined in terms of the LP modes, which can be written with the following dispersion relation [13, 14]:

$$u_{co}\frac{J_1(u_{co})}{J_0(u_{co})} = w_{co}\frac{K_1(w_{co})}{K_0(w_{co})} \tag{2}$$

where J_0 and J_1 are Bessel functions of the first kind, and K_0 and K_1 are the modified Bessel functions of the second kind of order zero and one, respectively. u_{co} and w_{co} are normalized transverse wave numbers. The relation between u_{co} and w_{co} is as follows [8, 12]:

$$w_{co}{}^2 = V^2 - u_{co}{}^2 \tag{3}$$

V-number is:

$$V = \frac{2\pi a_{co}}{\lambda}\sqrt{n_{co}^2 - n_{cl}^2} \tag{4}$$

where n_{co} and n_{cl} are the refractive index of the core and cladding, a_{co} is the radius of the core, and λ is wavelength.

u_{co} and w_{co} depend only on the fiber's physical parameters. After the fiber parameters for the core and cladding materials (radius and refractive indices at a given, -free space- wavelength) have been defined as the inputs, V-number is calculated from the Equation (4). Then, the eigenvalues that satisfy the dispersion relation are found graphically (using MATLAB): the left- and right-hand sides of the dispersion relation are plotted on the same set of axes, and the intersection point specify the eigenvalue of the dispersion relation and thus also the normalized transverse wave number (u_{co}). In our study, based on the fiber's parameters used, there was only one inter-section point (cf. Figure 3 (a)) (single-mode fiber).

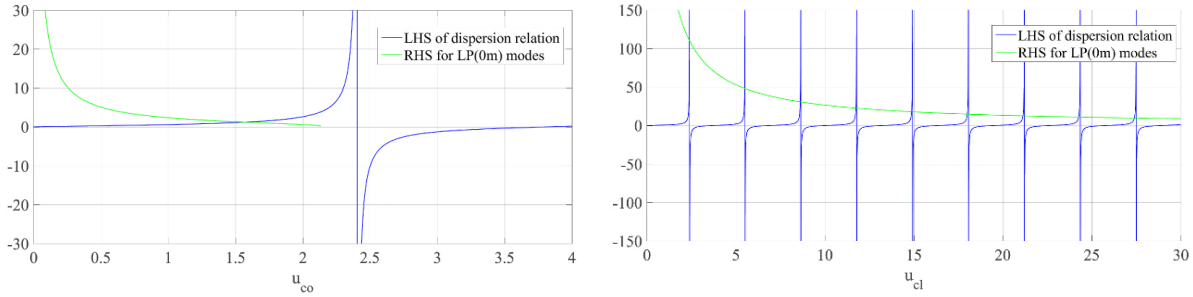

(a) **(b)**

Figure 3. (a) Determining the normalized transverse wave number (u_{co}) for core mode with graphical method; (b) Determining the $u_{cl}^{(m)}$ values for cladding modes.

The propagation constant of the fundamental core mode can be calculated from the fiber parameters (n_{co} and a_{co}), determined u_{co}, and the relevant free-space propagation constant (k) for each value of wavelength in the required range [15]:

$$\beta_{co} = \sqrt{(kn_{co})^2 - \left(\frac{u_{co}}{a_{co}}\right)^2} = \sqrt{\left(\frac{2\pi}{\lambda}n_{co}\right)^2 - \left(\frac{u_{co}}{a_{co}}\right)^2} \tag{5}$$

Finally, the effective refractive index of the core mode is obtained by using the following formula for each wavelength value in the wavelength interval of interest:

$$n_{eff\_co} = \frac{\beta_{co}}{k} = \frac{\beta_{co}\lambda}{2\pi} \tag{6}$$

$n_{cl} < n_{neff\_co} < n_{co}$ for the fundamental core mode [8, 12].

2.1.1.2. Effective refractive indices of cladding

Calculation of various cladding modes effective refractive indices is very similar to the procedure of determining the core effective refractive index. But in this case, the core region is ignored, while the cladding region is taken as the core region and the uniform external medium is considered as the new cladding (cf. Figure 2 (a)) [11]. In this way, a simple two-layer waveguide model is defined by using the fiber cladding and external medium. Based on this two-layer assumption, a new V-number is calculated from the equation given in (4), but taking into account in this particular case, $a_{co} = a_{cl}, n_{co} =$

n_{cl} and $n_{cl} = n_{ext}$: where n_{cl} and a_{cl} are the refractive index and the radius of the cladding, respectively; and n_{ext} is the refractive index of the external medium.

The LP mode dispersion relation in the form of an eigenvalue equation is used once again for finding each cladding mode propagation constant (Equation (2)). Left- and right-hand sides of the dispersion relation are plotted on the same set of axes again, but due to the larger fiber dimensions the graphical representation has different intersection points, and each intersection point specify one of several normalized transverse wave numbers ($u_{cl}^{(m)}$) belonging to a specific cladding mode (cf. Figure 3 (b)). The number of intersection points also corresponds to the number of cladding modes. The wave numbers corresponding to the two-layer cladding-ambient geometry are defined as follows [10]:

$$u_{cl}^{(m)} = a_{cl}\sqrt{k^2 n_{cl}^2 - \left(\beta_{cl}^{(m)}\right)^2} \tag{7}$$

$$w_{cl}^{m} = a_{cl}\sqrt{\left(\beta_{cl}^{(m)}\right)^2 - k^2 n_{next}^2} \tag{8}$$

The propagation constants belonging to the each m-order cladding mode ($\beta_{cl}^{(m)}$) are determined from the fiber's physical parameters (n_{cl}, a_{cl}) , calculated $u_{cl}^{(m)}$ values and the free-space propagation constant at specific wavelengths (k) [13]:

$$\beta_{cl}^{(m)} = \sqrt{(kn_{cl})^2 - \left(\frac{u_{cl}^{(m)}}{a_{cl}}\right)^2} = \sqrt{\left(\frac{2\pi}{\lambda}n_{cl}\right)^2 - \left(\frac{u_{cl}^{(m)}}{a_{cl}}\right)^2} \tag{9}$$

The cladding effective refractive indices of the m^{th} cladding modes can now be obtained with the following expresssion, for each wavelength value in the required range:

$$n_{eff\_cl}^{(m)} = \frac{\beta_{cl}^{(m)}}{k} = \frac{\beta_{cl}^{(m)}\lambda}{2\pi} \tag{10}$$

$n_{ext} < n_{eff\_cl}^{(m)} < n_{cl}$ for all the cladding modes [12].

2.1.2. Determining the coupling coefficients

The coupling coefficients for coupling between two co-propagated modes of azimuthal order v and μ can be determined by the formula given in Equation (11) [16]. The azimuthal order $\mu = 0$ for the fundamental core mode and the azimuthal order $v = 1$ for the m^{th} cladding modes.

$$\mathcal{K}_{v=1,\mu=0}^{(cl-co)}(z) = j\sqrt{2}\left[\frac{\gamma\left(\sqrt{\rho}\right)J_\mu(Ka_{co})\,J_v(\sigma a_{co})\sqrt{(n_{co}/n_{cl})-1}}{\pi a_{co}\sqrt{\left|J_{\mu-1}(Ka_{co})\,J_{\mu+1}(Ka_{co})\right|}}\right] \div \left|\sigma J_{v-1}(\sigma a_{co})H_v^{(1)}(\rho a_{co}) - \rho J_v(\sigma a_{co})H_{v-1}^{(1)}(\rho a_{co})\right| \tag{11}$$

where $H^{(1)}$ is a Hankel function of the first kind, and the other unknowns are as the following expressions [16]:

$$\sigma = \sqrt{n_{co}^2 k^2 - (\beta_{cl}^{(m)})^2} \tag{12}$$

$$\rho = \sqrt{n_{cl}^2 k^2 - (\beta_{cl}^{(m)})^2} \tag{13}$$

$$K = \sqrt{n_{co}^2 k^2 - {\beta_{co}}^2} \tag{14}$$

$$\gamma = \sqrt{{\beta_{co}}^2 - n_{cl}^2 k^2} \tag{15}$$

2.1.3. Determining the detuning parameter and the transmission spectrum

After the coupling coefficients are obtained for the entire wavelength range from Equation (11), the detuning parameters are determined from Equation (16) for each resonant wavelength in the wavelength interval.

$$\delta = \frac{1}{2}\left(\beta_{co} - \beta_{cl}^{(m)}\right) - \frac{\pi}{\Lambda} = \frac{\pi}{\Lambda\lambda}\left(\Delta n_{eff}\Lambda - \lambda\right) \tag{16}$$

where β_{co} and $\beta_{cl}^{(m)}$ are the propagation constant of the core mode and the m^{th}cladding mode, respectively. After implementing the long period fiber grating parameters to the final step of the code, the entire transmission spectrum of a single long period grating can be simulated from the Equation (17) [8, 12]:

$$T_{single} = cos^2\left(L\sqrt{\kappa_m^2 + \delta^2}\right) + \delta^2\left[\frac{sin^2\left(L\sqrt{\kappa_m^2 + \delta^2}\right)}{\kappa_m^2 + \delta^2}\right] \tag{17}$$

δ is detuning parameter for co-directional coupling, L is the length of the grating part, and κ_m is [12]:

$$\kappa_m = \frac{\Delta n}{2n_{co}} \times \mathcal{K}_{\nu=1,\mu=0}^{(cl-co)}(z) \tag{18}$$

Δn; induced core index change.

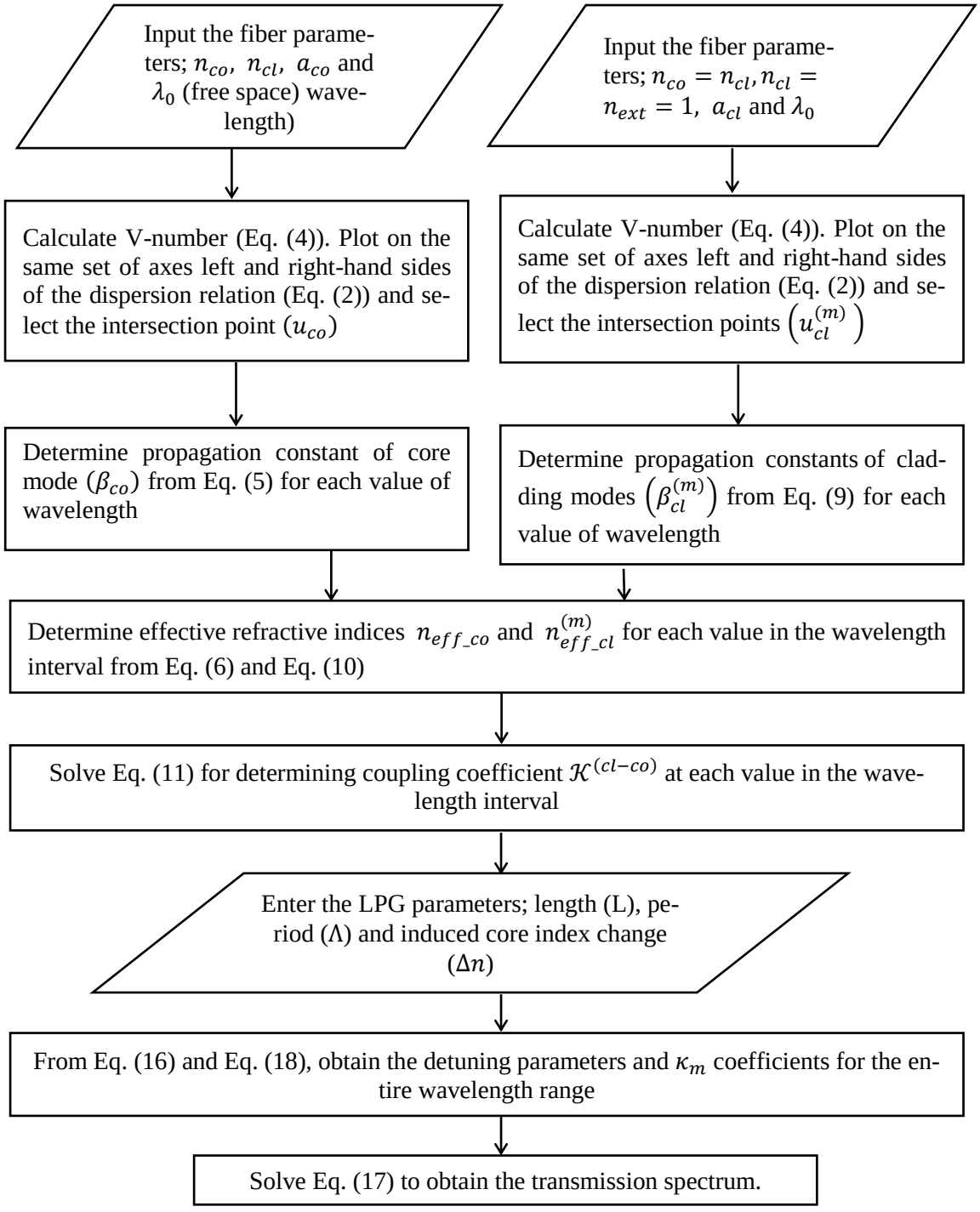

Figure 4. Flow-chart of the process used to determine the transmission spectrum of the LPFG in air ($n_{ext} = 1$).

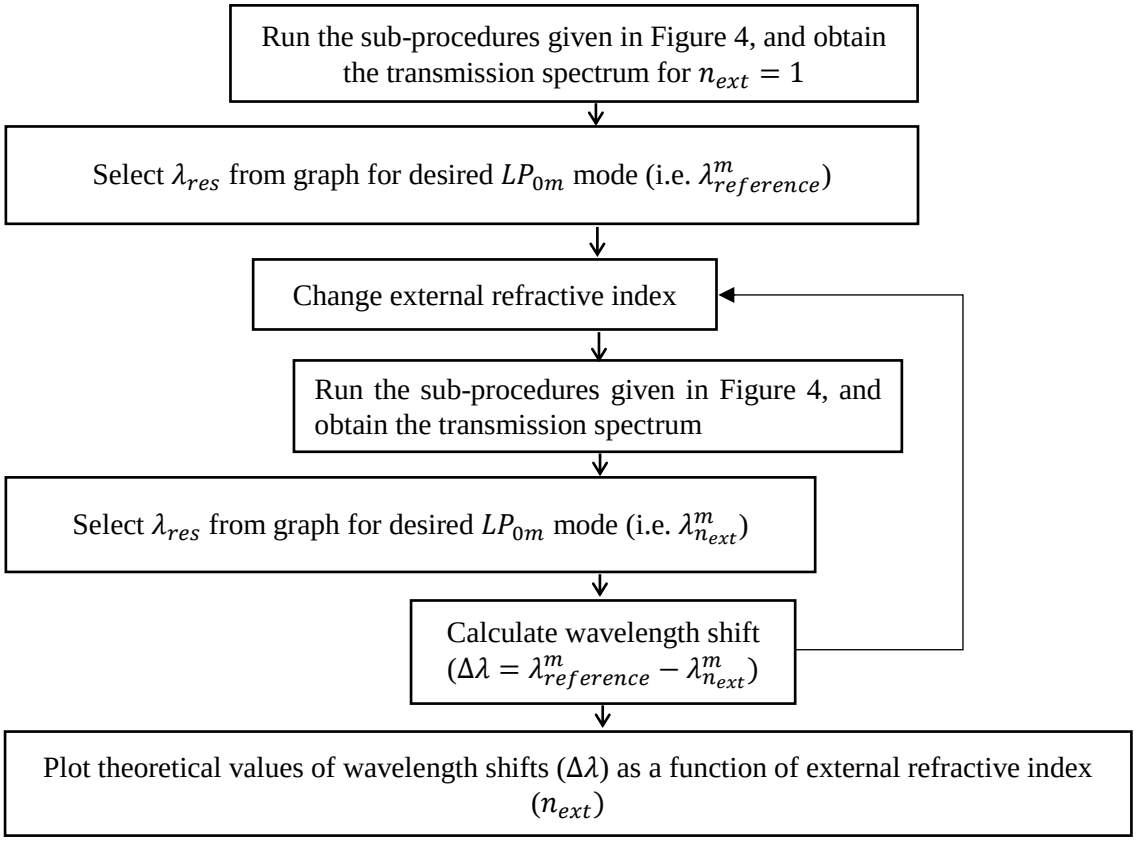

Figure 5. Flow-chart of the process used to determine the characteristic spectrum of the LPFG based on the different external refractive indices that are smaller than refractive index of the cladding.

2.2. Experiments

The layout of the experimental refractive index measurement system used to implement long period fiber grating as a sensor head is shown in Figure 6. It comprises a broadband light source, and an optical spectrum analyzer (OSA) to observe the transmission spectrum, and a personal computer for data acquisition and analysis.

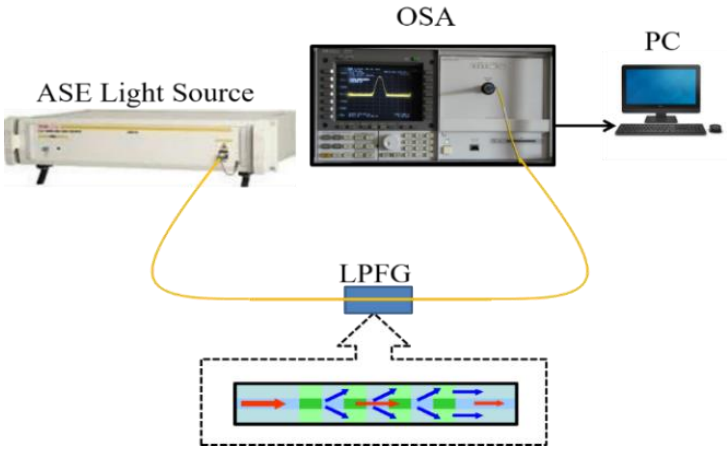

Figure 6. Schematic experimental setup.

LPFG sensors used in the experiments were fabricated and characterized by the Electromagnetism and Telecommunication Department, University of Mons (UMONS, Belgium) using a conventional single mode fiber (Corning SMF-28) and employing the point-by-point technique. The length of the fabricated grating part is 30 mm, and the grating period is 550 μm.

In the experimental set-up, one end of the fiber containing the LPG part was connected to the ASE light source while the other end connected to the optical spectrum analyzer to interrogate the transmission spectrum. LPFG sensor was fixed from two sides in a position where the transmission bands were clearly observed on the OSA. In this way, effects of strain and bending were avoided. Temperature of the laboratory was also recorded. All the experiments were realized at room temperature (25˚C ± 1˚C).

Glycerin (also called as glycerine or glycerol) - pure water solutions (prepared with 10% increments from concentration of 10% to 100%) were added dropwise on to the LPFG sensor part with the help of the dropper, and the transmission spectrums were recorded for different concentration samples. There was no protective coating on the grating part for sensing the physical changes. Hence, the effective refractive indices of the cladding modes were affected by the changes of the external refractive index. After each measurement with a given glycerin concentration value, sensor part was delicately cleaned with pure water. After removal of excess water, the transmission spectrum of LPFG was observed until it returned to the initial position (typically a few tens of seconds). Then, the same process was repeated with the successive sample having another concentration values. The spectrum of the LPFG in air ($n_{ext} = 1$) was selected as the reference spectrum for all the refractive index measurements. After each measurement, we ensured that the LPFG attenuation dip returns to the reference position.

When the measurements were completed, caps of all the test tubes which contained the chemicals were wrapped with *parafilm* to prevent any changes in the concentration values due to evaporation of water (the refractive index values depend on the percentage of glycerin and water in the samples).

During the time intervals between long-term repeatability measurements, the solutions were kept in a box at a dry place. For the second trial of the experiments (three months after the first trial) whole set of measurements were repeated. The measurement results were consistent with the first experiment set for all the chemicals, except 50% glycerin-pure water solution which was prepared again.

Experiments of the same type were realized with glucose - pure water solutions. The sugar solutions were prepared with 10% increments, from 10% to 50% concentration at the laboratories of Food Engineering Department of Izmir Institute of Technology.

The spectrum traces of the LPFG were acquired and recorded on a PC by using Keysight VEE Pro 9.32 (cf. Figure 7). The recorded data were analyzed by using a custom MATLAB routine. From the plotted graphics, the resonant wavelengths were determined for each measurement and wavelength shifts ($\Delta\lambda$) compared to the reference resonant wavelength were calculated. The characteristic response curve of the LPFG was determined based on the RI and $\Delta\lambda$ values.

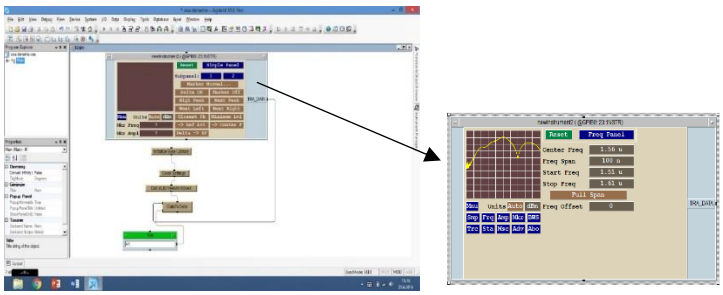

Figure 7. Keysight VEE Pro 9.32 interface software screenshots (before and during measurement).

After determining the experimental characteristic response curves (calibration curves) of the LPFG, the unknown refractive index values of the different solutions were determined depending on the wavelength shifts of the resonant wavelengths relative to the reference. For these RI measurements two new glycerine-distilled water solutions prepared at different concentration (65% and 77%) and argan oil were used.

The reference measurements presented in this work have been realized by using a state-of-the-art refractometer: RE50 (Mettler Toledo), having the light source at 589.3 nm. These reference values were then converted into values at the wavelength of 1550 nm, which constitutes one of the main contributions of our work. Conversion of the refractive indices of the chemicals at 589 nm wavelength to at 1550 nm was realized based on the refractive index values of distilled water and glycerin at 1550 nm[2] given by Saunders et. al. [18] by using:

$$n_R(\lambda) = \frac{\left(n_{pure\_glycerin}(\lambda) \times R\right) + \left(n_{water}(\lambda) \times (100 - R)\right)}{100} \tag{19}$$

where R is the ratio of glycerin in the solution.

2.2.1. Experimental results

The measured transmission spectrums of LPFG for different concentrations of glycerin-distilled water (Set-1 and Set-2) and sucrose-distilled water solutions are plotted on Figure 8, 9, and 10.

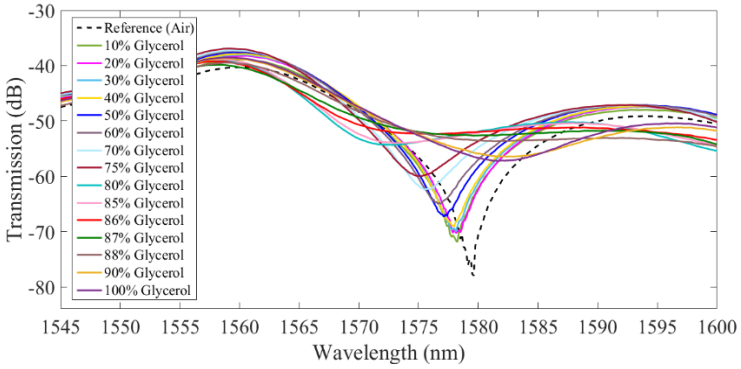

Figure 8. Changes in the transmission spectrum of the LPFG for glycerol-distilled water solutions at different concentrations (results for experiment Set-1).

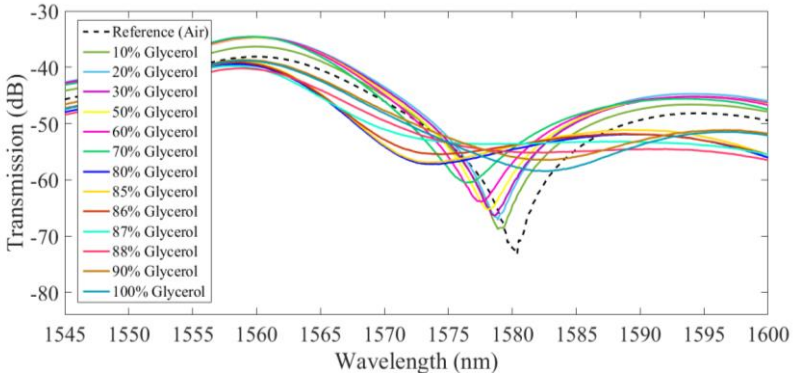

Figure 9. Changes in the transmission spectrum of the LPFG for glycerol-distilled water solutions at different concentrations (results for experiment Set-2).

[2] $n_{water} = 1.3164$ and $n_{pure\_glycerin} = 1.4571$ at λ=1550 nm.

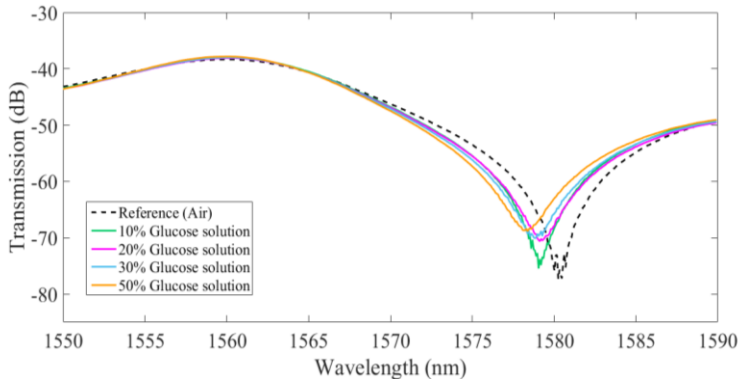

Figure 10. Changes in the transmission spectrum of the LPFG for glucose-distilled water solutions at different concentrations.

2.2.2. Enhancement of signal to noise ratio

In order to obtain an SNR enhancement on the measured spectra, "*smoothing operation*" was applied on all the measurements (cf. Figure 11).

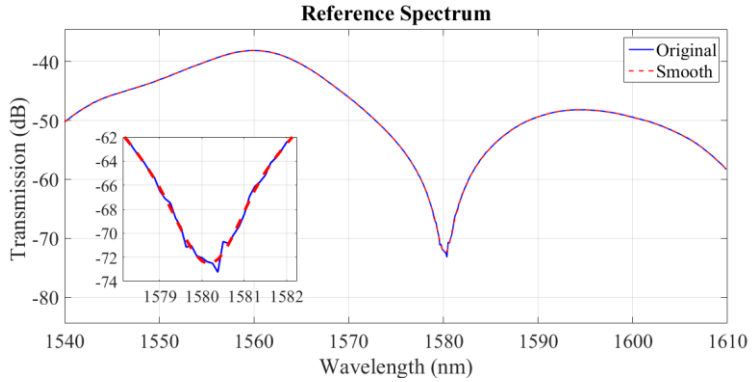

Figure 11. Comparison of the original and the smoothed signal. Inset: zoom on the attenuation dip.

Once the smoothing process was applied to the measured spectra, the derivatives of the signals were taken and the coordinates of the points passing through zero were determined. The dip points of the spectra corresponding to the resonant wavelength values have been determined in this way (cf. Figure 12 (b)).

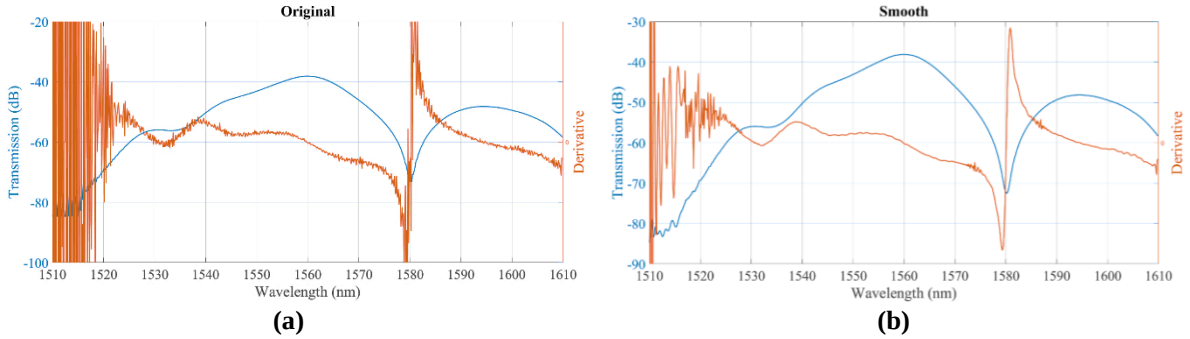

Figure 12. Derivative of the original reference (air) transmission spectrum; (a) Before, and (b) After smoothing process.

After determining the shifted resonant wavelength values observed for chemicals having different refractive index values, the wavelength shifts relative to the reference spectrum were calculated (initial wavelength being for the LPFG in air). The measured shift in resonant wavelength as a function of the

refractive index of the surrounding medium is represented in Figure 13 for glycerin-distilled water solutions Set-1 and 2.

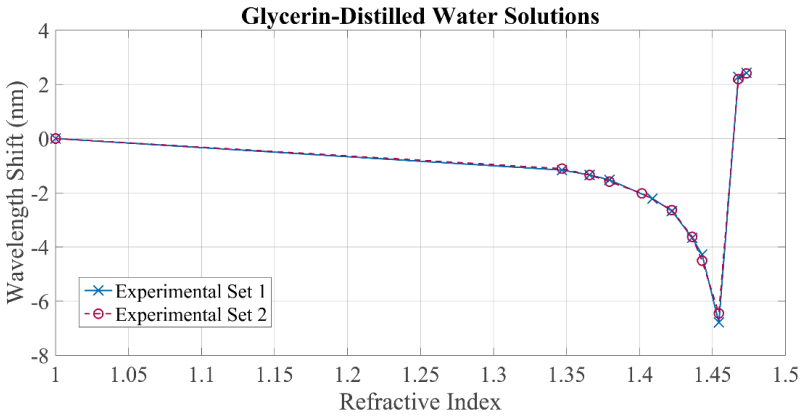

Figure 13. Wavelength shifts for glycerin-distilled water solutions for experiment Set-1 and 2 (measured with three months of time interval between them).

The wavelength shifts obtained for experimental Set-1 and Set-2 were consistent with each other (there were 3-months of time interval between two sets). This shows the results are reproducible. Small differences may be attributed to the bending sensitivity of the sensor and/or refractive index differences of the solutions due to the evaporation of water.

Experiments were also performed with glucose-distilled water solutions prepared from 10% to 50% (the concentration values of more than 50% were not prepared as the solutions would become saturated after a certain glucose ratio at room temperature). Higher wavelength shifts were observed for 30% and 50% glucose-distilled water solutions compared to the experiments with glycerin-distilled water solutions that have close refractive index values to these glucose solutions. This difference is interpreted as a result of the sugar crystals that may have accumulated on the fiber after each measurement.

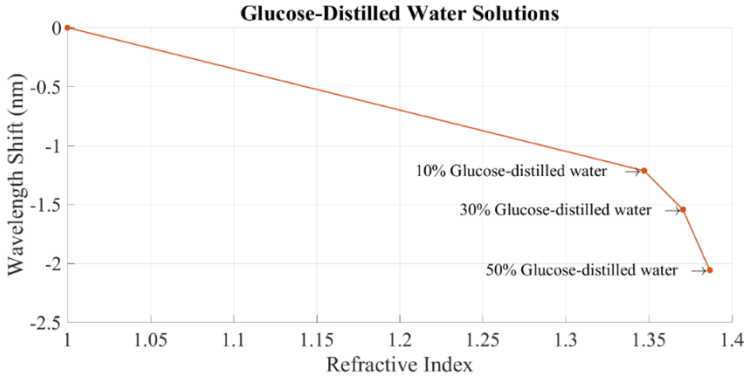

Figure 14. Wavelength shifts for glucose-distilled water solutions.

For finding the theoretical resonant wavelengths at different refractive index values, all the refractive index values of glycerin-water solutions were converted to the RI values at light source wavelength (1550 nm was considered as the free-space wavelength) (cf. Table 1). The theoretical spectrums were determined for LP_{04} linearly polarize modes (for the program flow-chart, cf. Figure 4). The simulation parameters to obtain the transmission spectrum of the LPFG written in a standard (*Corning*) SMF28 are given in Table 1.

Table 1. Parameters of standard single mode fiber and written LPFG.

Parameters	Symbols	Values
Core radius	a_{co}	4.1 μm
Cladding radius	a_{cl}	62.5 μm
Core refractive index[3]	n_{co}	1.4504
Cladding refractive index[4]	n_{cl}	1.4447
Free space wavelength	λ	1550 nm
Grating period	Λ	550 μm
Grating length	L	30 mm
Induced core refractive index change	Δn	$0.5x10^{-4}$

[3] Core refractive index was taken as 1.4504 (refractive index of Ge-doped fused silica at 1550 nm).
[4] Cladding refractive index was taken as 1.4447 (refractive index of fused silica at 1550 nm).

The wavelength shifts obtained for two experimental sets of glycerin-distilled water solutions and the corresponding theoretical values plotted on the same graph are shown in Figure 15. All the experimental and theoretical results were found to be highly compatible (cf. Figure 15 and Table 2) (except the slight difference between the experimental and theoretical wavelength shifts observed at 80% glycerin-distilled water solution (n_{ext} =1.4381 at 1550 nm). This can be attributed to the measurement errors due to the experimental difficulty of the wavelength detection due to the flattening of the spectra as the external refractive index approaches the refractive index of the cladding, and to the experimental deviation from theoretical values due to the radiation modes occurred in this range. The other small deviations may be attributed to the fixed position of the LPFG, where it is slightly inclined. This bending may have caused some additional wavelength shifts by increasing the sensitivity of the sensor to the external refractive index due to the increased evanescent wave interaction.

Table 2. Experimental and the theoretical values.

Chemicals	n (λ) at 589.3 nm	n (λ) at 1550 nm	Theoretical Δλ (nm) of LP_{04} mode	Experimental Δλ (nm) of LP_{04} mode (Set-1)	Experimental Δλ (nm) of LP_{04} mode (Set-2)
Air	1	1	0	0	0
10% glycerol	1.34703	1.3305	- 1.102	- 1.165	- 1.114
20% glycerol	1.36587	1.3494	- 1.304	- 1.346	- 1.347
30% glycerol	1.37943	1.3630	- 1.502	- 1.526	- 1.592
50%[5] glycerol	1.40163	1.3852	- 1.956	-	- 2.025
50% glycerol	1.40900	1.3926	- 2.155	- 2.219	-
60% glycerol	1,42228	1.4059	- 2.705	- 2.674	- 2.647
70% glycerol	1,43612	1.4198	- 3.655	- 3.666	- 3.627
75% glycerol	1,44291	1.4266	- 4.455	- 4.284	- 4.512
80% glycerol	1,45441	1.4381	- 7.601	- 6.790	- 6.452
85% glycerol	1.45462	1.4383	-	-	-
86% glycerol	1.45502	1.4388	-	-	-
87% glycerol	1.45758	1.4413	-	-	-
88% glycerol	1.45969	1.4434	-	-	-
90% glycerol	1.46777	1.4515	-	2.274	2.194
Pure glycerol	1.47332	1.4571	-	2.424	2.406

[5] 50% glycerol solution: this solution was different for experiment one and experiment two. For the second experimental sets this solution was prepared again and its refractive index was measured with a RE50 digital refractometer ($n_{ext\_50\%} = 1.40163$). For the first one, the refractive index of the solution was 1.40900.

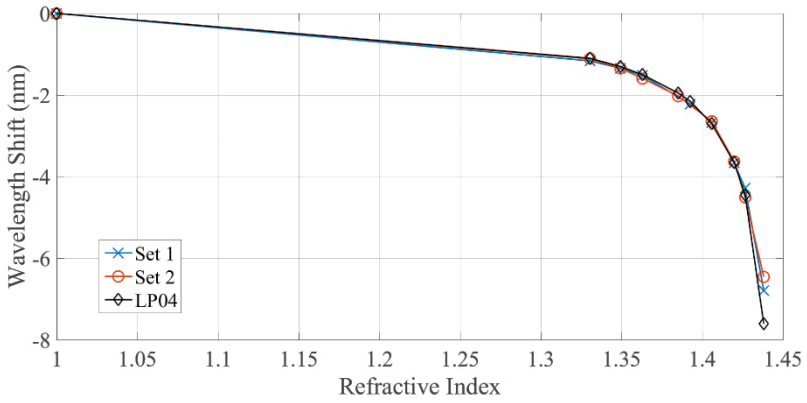

Figure 15. Comparison of experimental (Set-1 and Set-2) and theoretical (LP_{04}) resonant wavelength shifts.

The highest sensitivity determined with the sensor was of 217.913 nm/RIU obtained in the RI range of 1.44291-1.45441. The resolution of the sensor was calculated as 4.6×10^{-4} depending on the resolution of the interrogator[6].

Results for refractive index measurement experiments are given in Table 3, 4 and 5.

Table 3. Resonant wavelength values and wavelengths shifts.

Chemical	λ_{res} (nm)	$\Delta\lambda$ (nm)
Air (reference)	1579.453	0
Argan oil	1577.583	- 1.870
65% glycerol solution	1576.051	- 3.402
77% glycerol solution	1574.948	- 4.505

Table 4. Comparison of the LPFG sensor-deduced refractive index vs reference RI for three chemicals.

Chemicals	Measured RIs (RE50 refractometer)	Calculated RIs from characteristic spectrums		
		Set-1	Set-2	Theoretical
Argan oil	1.39910	1.3941	1.3937	1.3974
65% glycerin	1.42819	1.4324	1.4329	1.4324
77% glycerin	1.44574	1.4439	1.4429	1.4431

Table 5. RI difference between LPFG sensor-deduced RI value and the reference value (RE50 digital refractometer).

Chemicals	$\lvert\Delta n\rvert$		
	Set-1	Set-2	Theoretical
Argan oil	5.0×10^{-3}	5.4×10^{-3}	1.7×10^{-3}
65% glycerin	4.2×10^{-3}	4.7×10^{-3}	4.2×10^{-3}
77% glycerin	1.8×10^{-3}	2.8×10^{-3}	2.6×10^{-3}

In the last step of the experiments, refractive index measurements were realised with the proposed LPFG-based RI sensor for three different solutions (65% and 77% glycerine-distilled water solutions and argan oil). The refractive index values of the solutions were determined by using the experimental

[6] Calculation of resolution [17]:

$$Resolution_{sensor} = Resolution_{OSA} \times (gradient)^{-1}$$
$$Resolution_{sensor} = 0.1\ nm \times (217.91\ nm/RIU)^{-1} = 4.6 \times 10^{-4}.$$

and theoretical characteristic response curves, depending on the wavelength shifts for each solution compared to the reference spectrum ($n_{ex} = 1$).

Experimental (Set-1 and Set-2) and theoretical spectra together with the reference RIs were plotted at 589 nm (rather than at 1550 nm). Hence, the RI values measured with the digital refractometer may easily be compared with the values measured with the LPFG sensor without any further transformation. The determined refractive index values of the solutions were found very close to the reference values measured with the RE50 digital refractometer (cf. Table 4 and 5). The differences between the values were in the third digit after the decimal point.

3. CONCLUSION

The optical fiber sensors have been fast becoming popular in many new application areas (e.g. food industry, environmental analysis and biomedical applications, etc.). In most of such domains, the C- and L-bands, commonly used for the telecommunication applications are being implemented as the commercial optoelectronic devices are readily available in these bands with reasonable prices. The measurement of refractive indices of common solvents in the 1550-1620 nm range is thus becoming critical for the new sensing and monitoring systems [19, 20]. In spite of the clear interest in RI calibration measurements for the corresponding RI sensors to be operated at the low attenuation windows, there is a very limited number of works reporting reliable refractive index values of organic solvents.

In this context, we report new measurements of refractive indices of common solvents and solutions at the telecommunication wavelength range using LPFG-based technique. As a first step, the surrounding refractive index sensitivity of the LPFG as a function of wavelength was investigated by the way of numerical analysis based on the coupled mode theory. Then, the experimental demonstration of the analyzed system has been realized on different concentrations of organic solvents providing a maximum sensitivity of 217.9 nm/RIU. We achieved a very good agreement between numerical and experimental results, that successfully demonstrated the capability of the LPFG sensor in measuring RI of liquids

ACKNOWLEDGEMENT

The authors would like to thank Dr. Damien Kinet and Dr. Christophe Caucheteur (University of Mons, Belgium) for the fabrication of long period fiber gratings used in this work and Dr. Burcu Okuklu (IZ-TECH Food Engineering Department) for reference RI measurements using conventional refractometer. Kıvılcım Yüksel acknowledges 2016-IYTE-50 BAP.

REFERENCES

[1] Alvarez-Herrero A, Guerrero H, Levy D. High-sensitivity sensor of low relative humidity based on overlay on side-polished fibers. IEEE, Sens J 2004; 4 (1): 52-56.

[2] Caucheteur C. Realization of mechanical and chemical sensors based on the fiber Bragg gratings technology, PhD, Faculté polytechnique de Mons, Mons, Belgium, 2007.

[3] Caucheteur, C, Tuan G, Fu, Bai-Ou G, Jacques A. Ultrasensitive plasmonic sensing in air using optical fibre spectral combs. Nature Comm 2016; 7 (13371).

[4] Del Villar I. Ultrahigh-sensitivity sensors based on thin-film coated long period gratings with reduced diameter, in transition mode and near the dispersion turning point. Opt Express 2015; 23 (7): 8389-8398.

[5] Coelho L, Viegas D, Santos JL, de Almeida JMMM. Characterization of zinc oxide coated optical fiber long period gratings with improved refractive index sensing properties. Sens Actuators B Chem 2016; 223 (0925-4005): 45-51.

[6] Coelho L, Viegas D, Santos JL, de Almeida JMMM. Enhanced refractive index sensing characteristics of optical fibre long period grating coated with titanium dioxide thin films. Sens Actuators B Chem 2014; 202 (0925-4005): 929-934.

[7] Garg R, Tripathi SM, Thyagarajan K, Bock W. J. Long period fiber grating based temperature-compensated high performance sensor for bio-chemical sensing applications. Sens Actuators B 2014, 176: 1121-1127.

[8] Erdogan T. Cladding-mode resonances in short- and long-period fiber grating filters. J Opt Soc Am A 1997; 14 (8): 1760-1773.

[9] Lee BH, Liu Y, Lee SB, Choi SS, Jang JN. Displacements of the resonant peaks of a long-period fiber grating induced by a change of ambient refractive index. Opt Lett 1997; 22 (23): 1769-1771.

[10] Hou R, Ghassemlooy Z, Hassan A, Lu C, Dowker KP. Modelling of long-period fibre grating response to refractive index higher than that of cladding. Meas Sci Technol 2001; 12 (10): 1709-1713.

[11] Vengsarkar AN, Lemaire PJ, Judkins JB, Bhatia V, Erdogan T, Sipe JE. Long-period fiber gratings as band-rejection filters. J Lightw Technol 1996; 14 (1): 58-65.

[12] Erdogan T. Fiber grating spectra. J Lightw Technol 1997; 15 (8): 1277-1294.

[13] Van Brakel A. Sensing characteristics of an optical fibre long-period grating Michelson refractometer. PhD, Rand Afrikaans University, Johannesburg, South Africa, 2004.

[14] Marcuse D, Gloge D, Marcatili EA. Guiding properties of fibres. Optical fiber telecommunications. New York: Academic Press, 1979.

[15] Jones WB. Introduction to Optical Fiber Communications Systems. UK: Oxford University Press, 1995.

[16] Marcuse D. Theory of Dielectric Optical Waveguides. 2nd ed. New York, USA: Academic Press, 1991.

[17] Yong D, Yu X, Ren G, Zhang H, Zhang Y, Chan CC, Wei H, Tong W. Photonic Bandgap Fiber for Infiltration-Free Refractive-Index Sensing, IEEE J Select Top Quant Electron 2012; 18 (5): 1560-1565.

[18] Saunders JE., Sanders C, Chen H, and Loock HP. Refractive indices of common solvents and solutions at 1550 nm. 2016 Appl. Opt., 55, 947-953.

[19] Ranjan R, Esposito F, Campopiano S, Iadicicco A. Arc-Induced Long Period Gratings: Analysis of the Fabrication Parameters on the Surrounding Refractive Index Sensitivity. In: Bhattacharya I, Chakrabarti S, Reehal H, Lakshminarayanan V. (eds) Adv in Opt Sci and Eng. Springer Proceedings in Physics, vol 194. Singapore: Springer, 2017.

[20] Lacraz A, Theodosiou A, Kalli K. Femtosecond laser inscribed Bragg grating arrays in long lengths of polymer optical fibres; a route to practical sensing with POF. E Let 2016; 52 (19): 1626 – 1627.